Supplementary Materials

Electrocatalytic CO₂ reduction to CO enabled by Ni-N_x high activity sites formed

by three-dimensional porous foams

Anqi Wei^{1,#}, Yang Xu^{1,#}, Jiangfang Wang¹, Lei Shi¹, Chong Wang^{1,*}, Yingjie Wu^{2,*},

Song Liu^{1,*}

¹College of Chemistry, Chemical Engineering and Resource Utilization, Northeast

Forestry University, Harbin 150040, Heilongjiang, China.

²School of Medicine and Health, Harbin Institute of Technology, Harbin 150001,

Heilongjiang, China.

*Authors contributed equally.

*Correspondence to: Prof. Dr. Liu Song and Prof. Dr. Chong Wang, Chemical

Engineering and Resource Utilization, Northeast Forestry University, No. 26 Hexing

Xiangfang District, Harbin 150040, Heilongjiang, China. E-mail: Road.

carlosliusong@nefu.edu.cn, wangchong@nefu.edu.cn; Prof. Dr. Yingjie Wu, School of

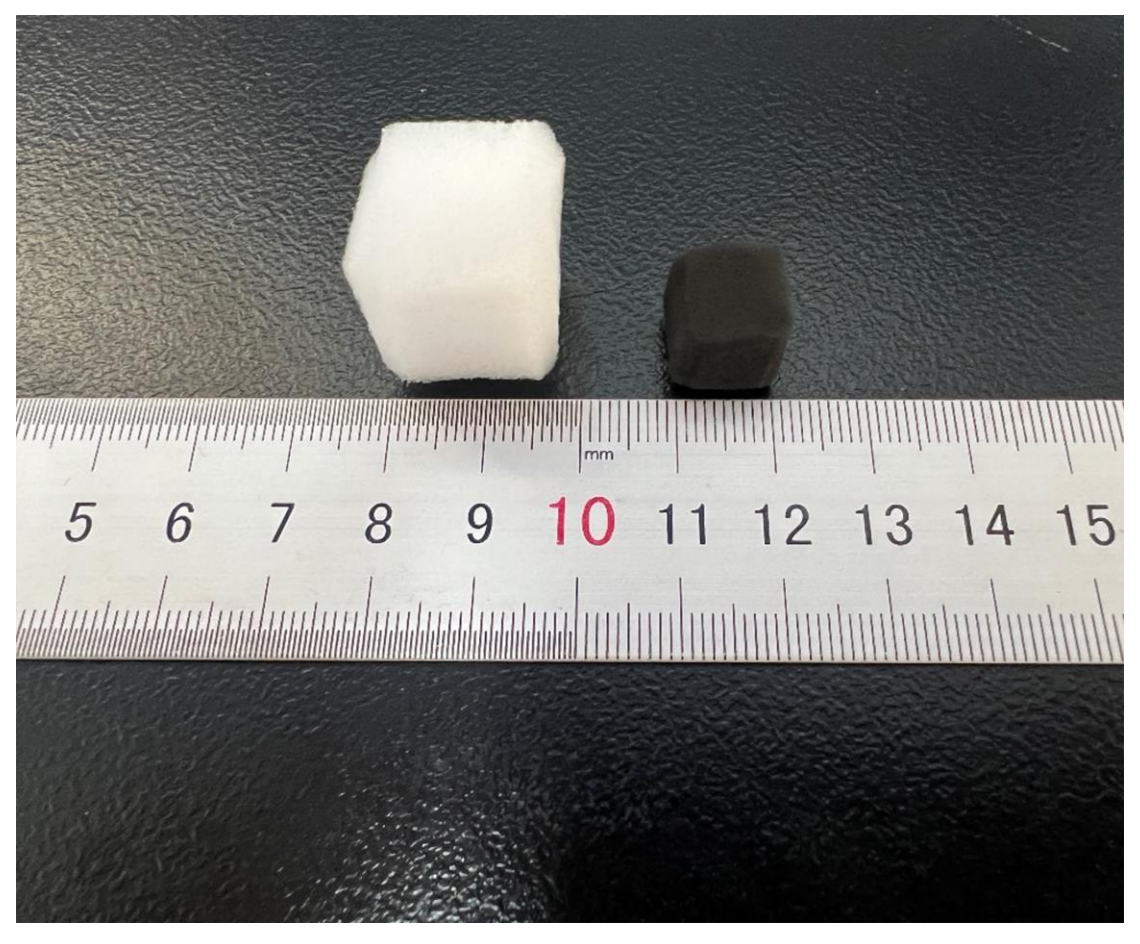
Medicine and Health, Harbin Institute of Technology, No. 92 Xidazhi Street, Nangang

District, Harbin 150001, Heilongjiang, China. E-mail: wuyingjie@hit.edu.cn

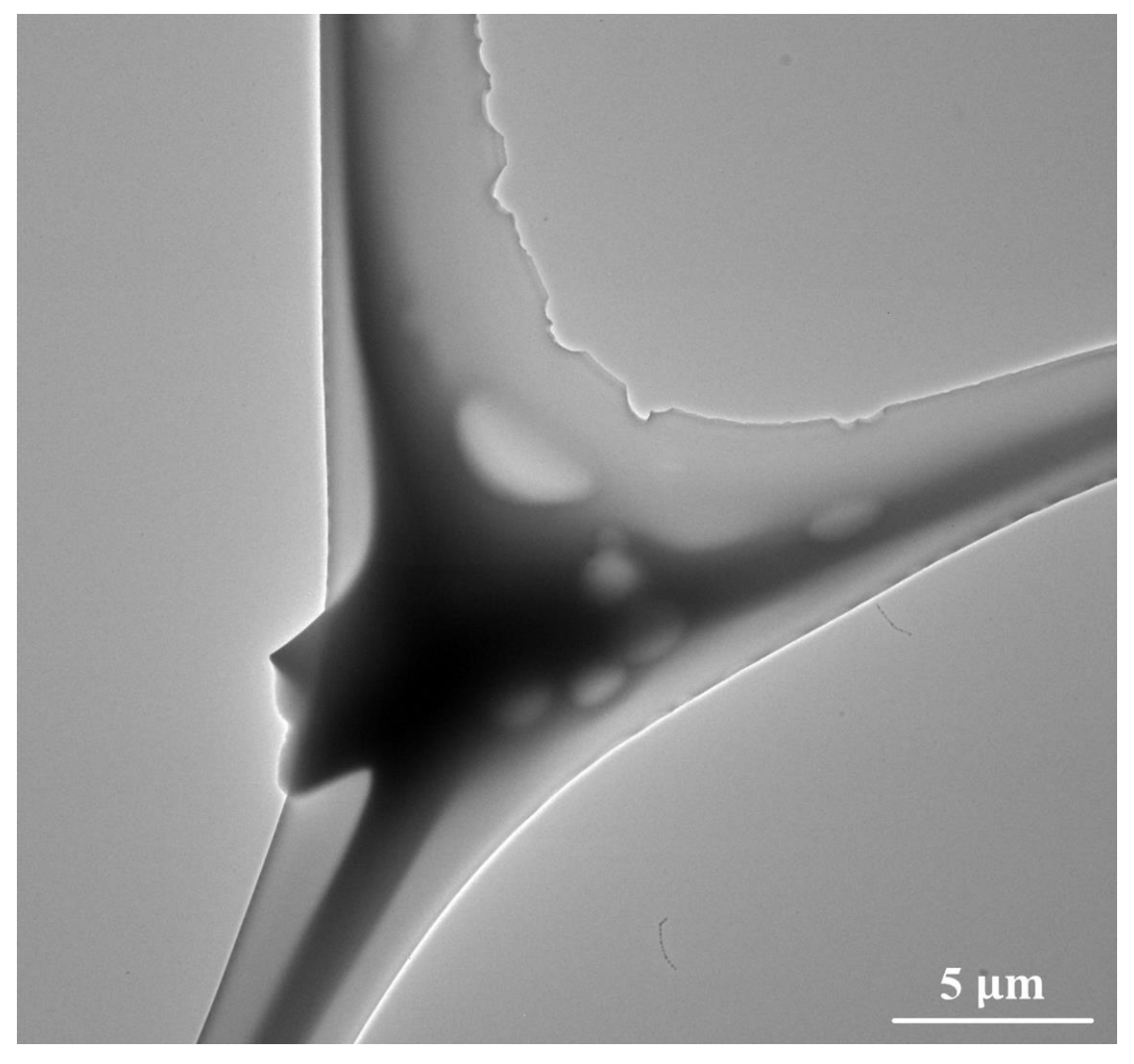
ORCID: Yingjie Wu (0000-0003-2480-257X)

S1

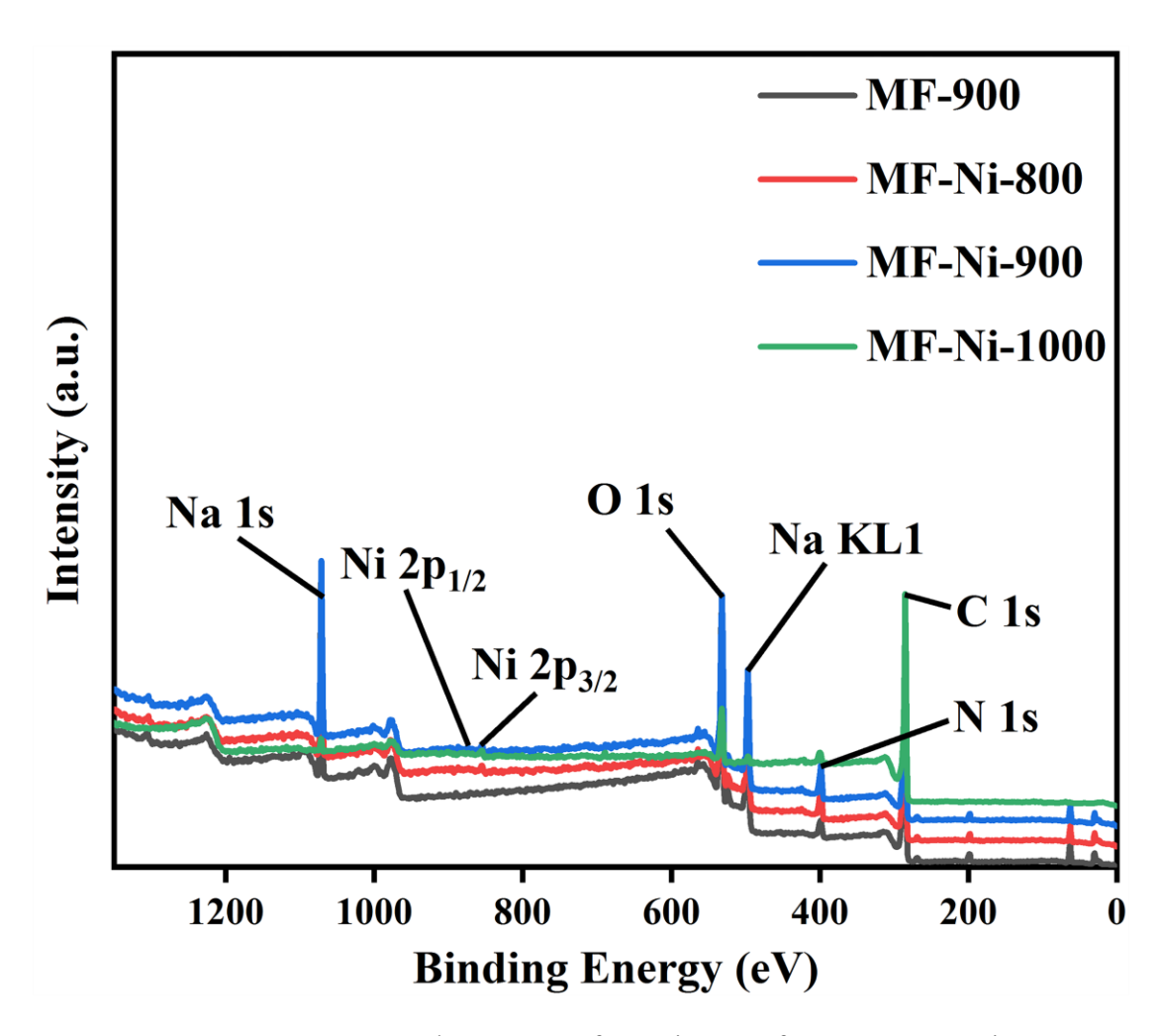
SUPPLEMENTARY FIGURES



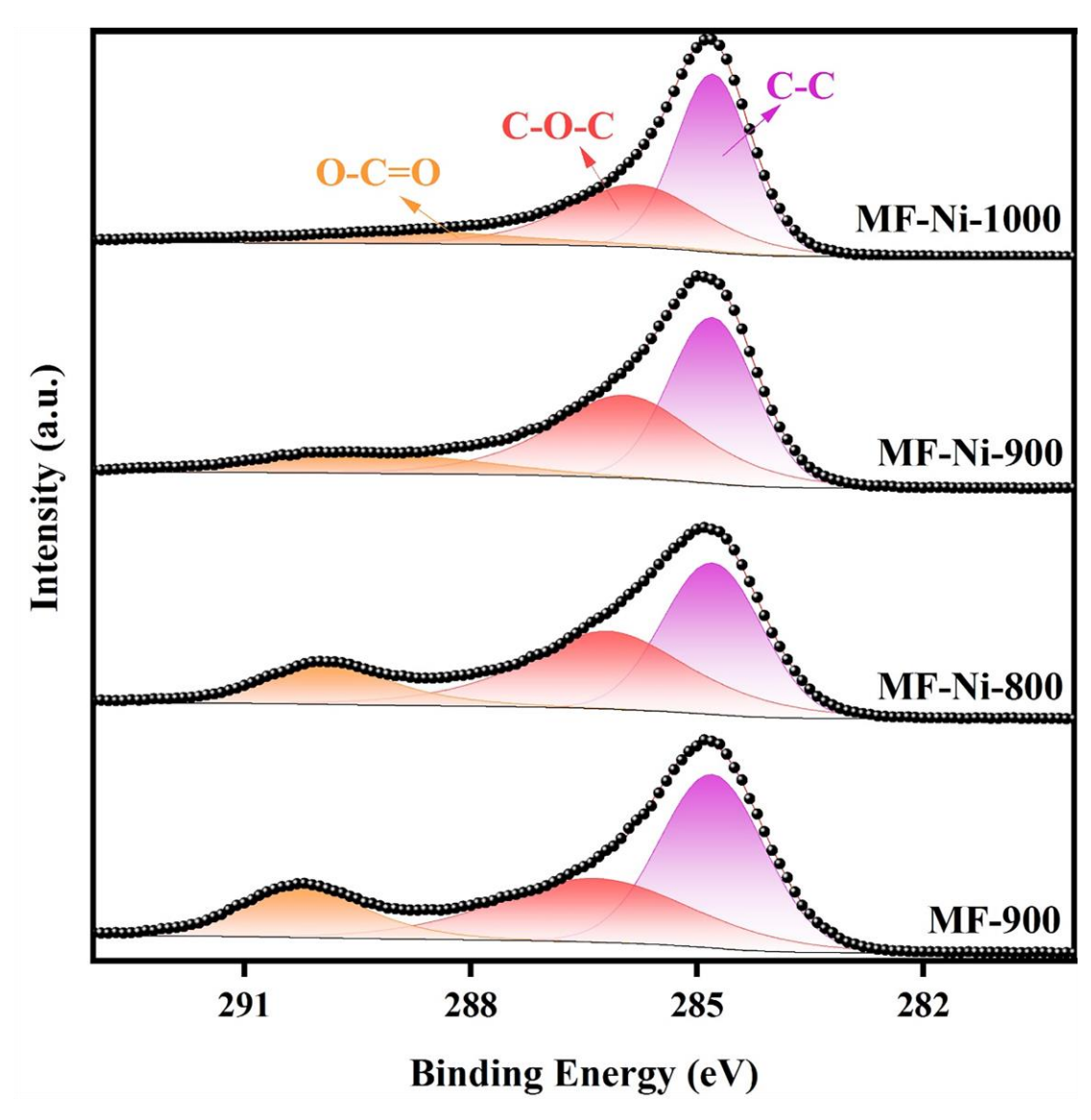
Supplementary Figure 1. Comparison of melamine foam volume before and after carbonization.



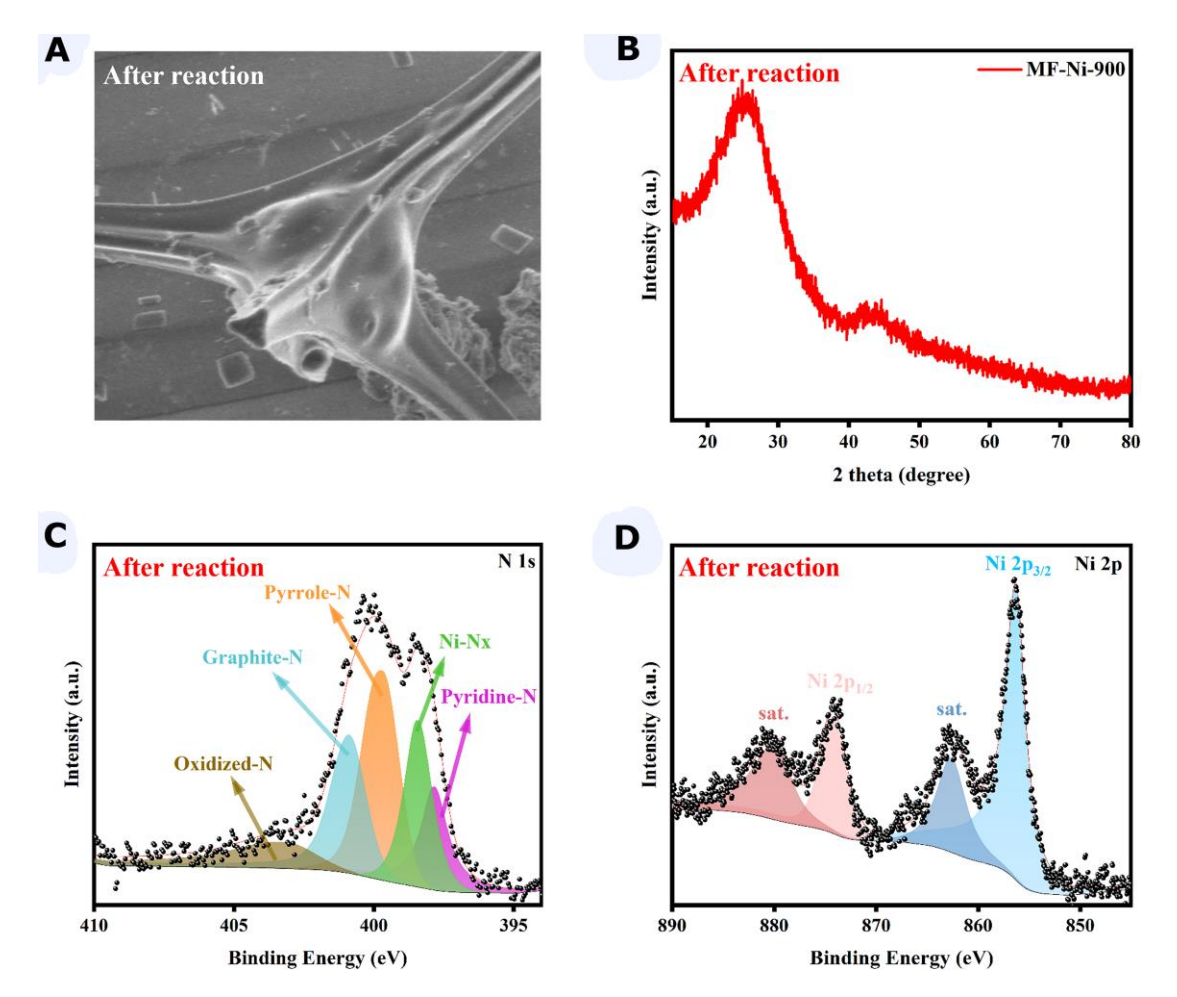
Supplementary Figure 2. HR-TEM image of MF-900 at 5 μm scale.



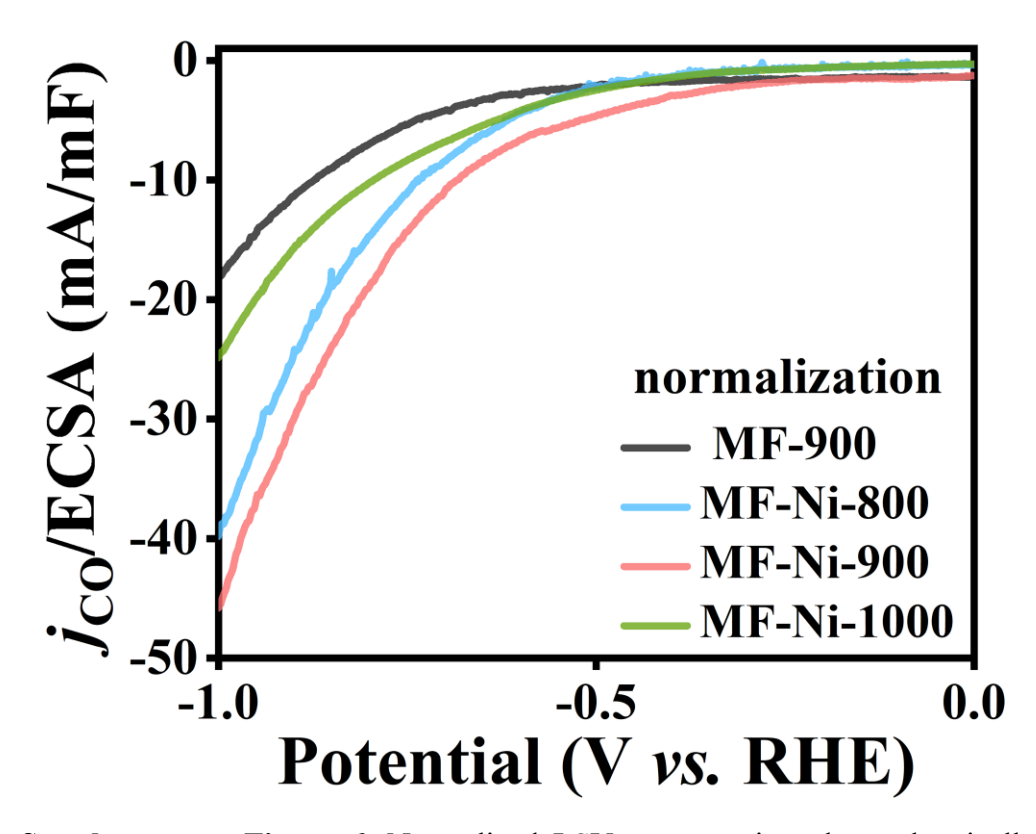
Supplementary Figure 3. Total spectrum of XPS image of MF-900, MF-Ni-800, MF-Ni-900, and MF-Ni-1000.



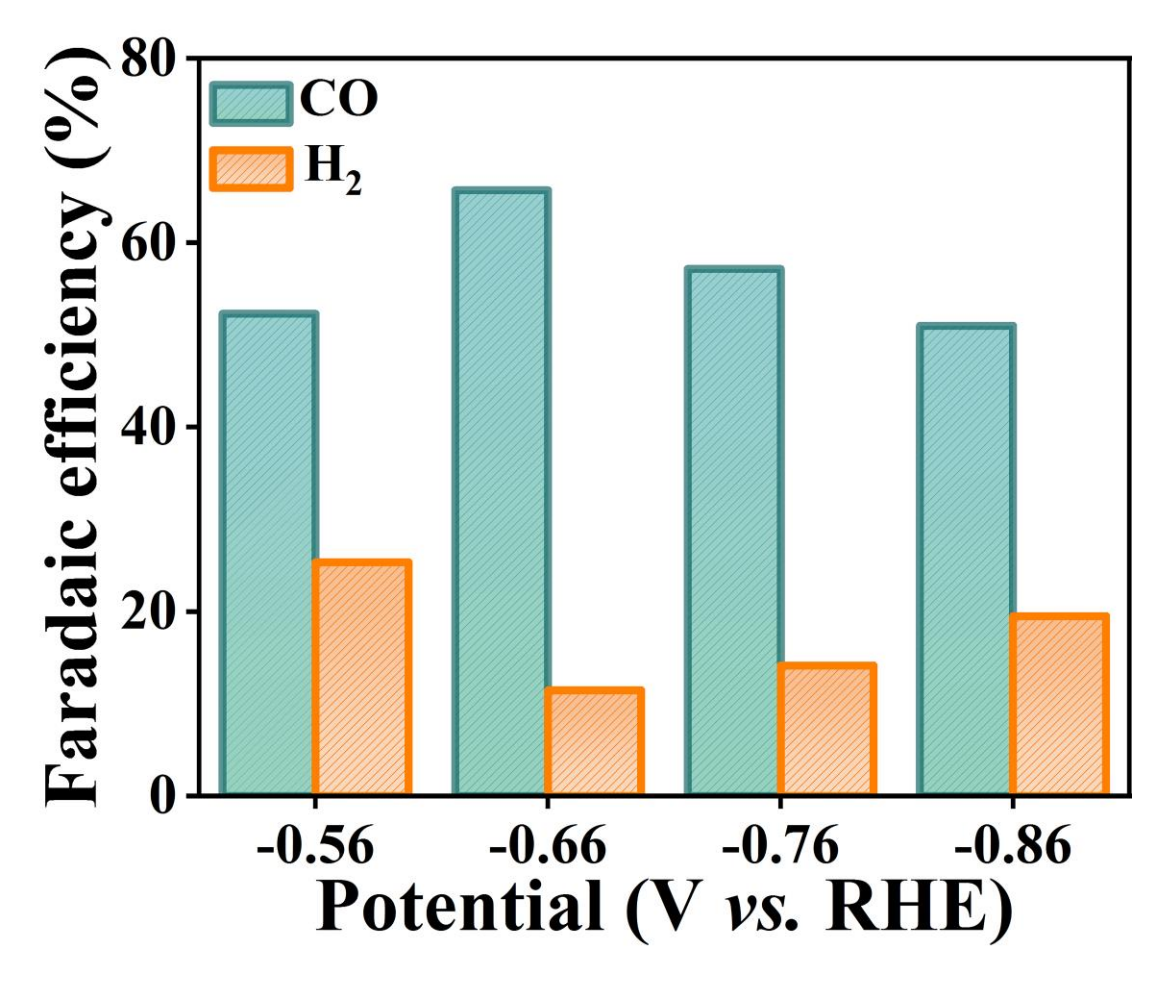
Supplementary Figure 4. C 1s spectrum of XPS image of MF-900, MF-Ni-800, MF-Ni-900, and MF-Ni-1000.



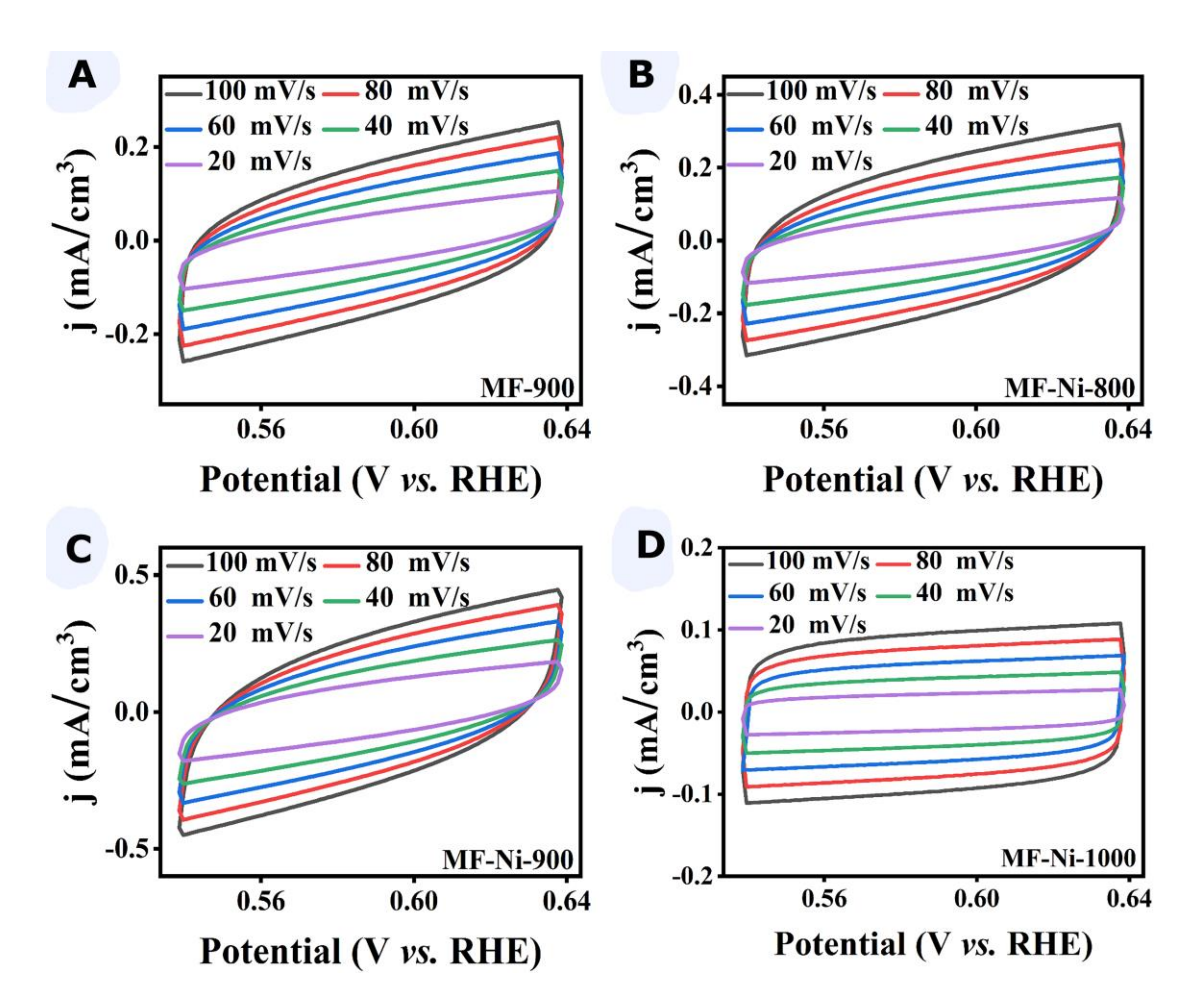
Supplementary Figure 5. (A-D) SEM image (A), XRD image (B), XPS N1s image (C), XPS Ni 2p image (D) of MF-Mi-900 after reaction.



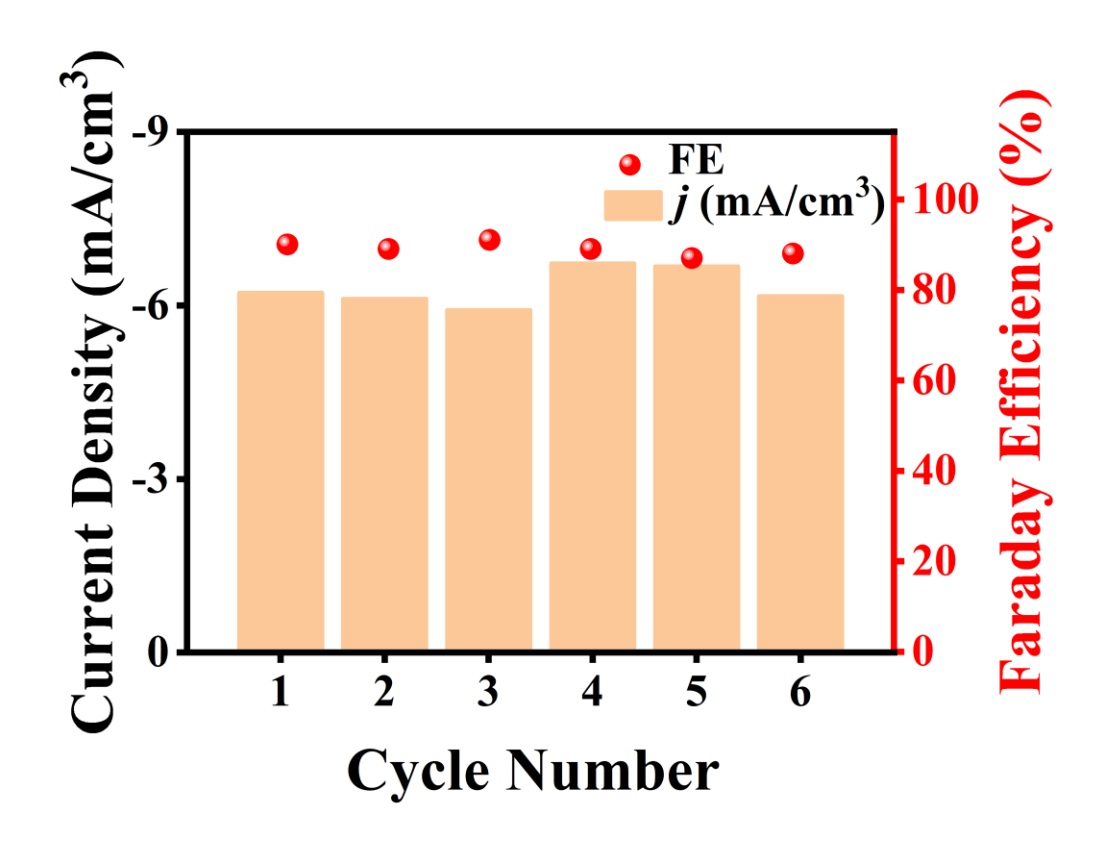
Supplementary Figure 6. Normalized LSV curves using electrochemically active specific surface area (ECSA).



Supplementary Figure 7. Faradaic efficiency plots of melamine powder loaded Ni monoatomic catalysts at different potentials.



Supplementary Figure 8. (A-D) ECSA images of MF-900 (A), MF-Ni-800 (B), MF-Ni-900 (C), and MF-Ni-1000 (D).



Supplementary Figure 9. 6 cycles stability test of MF-Ni-900.

SUPPLEMENTARY TABLES
Supplementary Table 1. Changes in mass (m) and volume (V) of the sample before and after carbonization

Catalysts	Before carbonization		After carbonization		
	V (mm ³)	m (mg)	V (mm ³)	m (mg)	
MF-900	19.0*20.0*21.0	50	12.0*10.0*9.0	8.5	
MF-Ni-800	20.0*20.0*19.0	50	11.0*11.0*8.0	8.5	
MF-Ni-900	21.0*20.0*20.0	50	10.0*9.0*11.0	8.8	
MF-Ni-1000	22.0*19.0*20.0	50	10.0*12.0*9.0	8.8	

^a No notable alteration was observed in the volume of the four samples prior to and following immersion. ^b The discrepancy in volume prior to charring could be attributed to the variation in foam cut.

Supplementary Table 2. Sample content analysis

XPS (%)	MF-900	MF-Ni-800	MF-Ni-900	MF-Ni-1000
Ni	-	1.85	2.38	1.86
C	65.15	65.38	65.31	78
N	23.41	26.67	26.25	24.49

^a The total C, N, and Ni content of less than 100 percent was due to the presence of residual oxygen (due to functional groups in formaldehyde or adsorbed H₂O and CO₂ added during the manufacture of MF), sodium (sodium hydroxide is added to adjust the pH of the solution during the manufacture of MF), and hydrogen (present in carbonized MF and adsorbed H₂O).

Supplementary Table 3. Types and content of N in XPS

XPS (%)	MF-900	MF-Ni-800	MF-Ni-900	MF-Ni-1000
Pyridine-N	9.11	8.75	5.71	5.8
Ni-Nx	-	5.85	9.47	3.95
Pyrrole-N	6.61	5.3	4.23	5.86
Graphite-N	5.37	5.25	4.92	7.18
Oxidized-N	2.32	1.52	1.92	1.7

Supplementary Table 4. Comparison of common catalyst properties

Materials	Electrolyte	E/V v	vs.	Product	FE	j (mAcm ⁻²)
		RHE			(%)	
Ni-N-CNS _S ^[1]	0.1 mol/L KHCO ₃	-0.85		СО	97.1	3.1
Fe/ZIF-8 ^[2]	0.1 mol/L KHCO ₃	-0.73		CO	85	3.7
Fe-N-C ^[3]	0.1 mol/L KHCO ₃	-0.6		CO	91	7.5
Fe _X N@Fe-N-	0.5 mol/L KHCO ₃	-0.53		CO	95	4.71
$C^{[4]}$						
Fe-N ₄ -	0.1 mol/L KHCO ₃	-0.6		CO	80	2.5
graphene ^[5]						
Fe-N-C ^[6]	0.5 mol/L KHCO ₃	-0.53		CO	95	1.9
Sb-NC ^[7]	0.1 mol/L KHCO ₃	-0.9		CO	82	2.4
Ni/Fe-N-C ^[8]	0.5 mol/L KHCO ₃	-0.7		CO	98	9.5

REFERENCES

- 1. Ma, Z.; Zhang, X.; Wu, D.; et al. Ni and nitrogen-codoped ultrathin carbon nanosheets with strong bonding sites for efficient CO₂ electrochemical reduction. *J. Colloid. Interface Sci.* **2020**, *570*, 31-40. DOI PubMed
- 2. Sun, X.; Wang, R.; Ould-Chikh, S.; et al. Structure-activity relationships in metal organic framework derived mesoporous nitrogen-doped carbon containing atomically dispersed iron sites for CO₂ electrochemical reduction. *J. Catal.* **2019**, *378*, 320-30. DOI
- 3. Huan, T.N.; Ranjbar, N.; Rousse, G.; et al. Electrochemical reduction of CO₂ catalyzed by Fe-N-C materials: a structure-selectivity study. *ACS Catal.* **2017,** *7*, 1520-5. DOI
- 4. Cheng, Q.; Mao, K.; Ma, L.; et al. Encapsulation of iron nitride by Fe-N-C shell enabling highly efficient electroreduction of CO₂ to CO. *ACS Energy Lett.* **2018**, *3*, 1205-11. DOI
- 5. Zhang, C.; Yang, S.; Wu, J.; et al. Electrochemical CO₂ reduction with atomic iron-dispersed on nitrogen-doped graphene. *Adv. Energy Mater.* **2018**, *8*, 1703487. DOI
- 6. Wu, S.; Lv, X.; Ping, D.; et al. Highly exposed atomic Fe-N active sites within carbon nanorods towards electrocatalytic reduction of CO₂ to CO. *Electrochim. Acta* **2020**, *340*, 135930. DOI
- 7. Jia, M.; Hong, S.; Wu, T.S.; Li, X.; Soo, Y.L.; Sun, Z. Single Sb sites for efficient electrochemical CO₂ reduction. *Chem. Commun.* **2019**, *55*, 12024-7. DOI PubMed
- 8. Ren WH, Tan X, Yang WF, et al. Isolated diatomic Ni-Fe metal-nitrogen sites for synergistic electroreduction of CO₂. *Angew. Chem. Int. Ed. Engl.* **2019**, *58*, 6972-6. DOI PubMed